


# Epitaxial growth of quasi-one-dimensional $TaNi_2Se_2$ monolayer with anisotropic electronic and mechanical properties

Jiayi Wang(王嘉翌), Qiuchen Yu(余秋辰), Hui Guo(郭辉), Peng Fan(范朋), Siyu Xu(徐思宇), Yixuan Gao(高艺璇), Hui Chen(陈辉), and Hong-Jun Gao(高鸿钧)

**Citation:**Chin. Phys. B, 2026, 35 (**7**): 077303. DOI: 10.1088/1674-1056/ae5a15
http://cpb.iphy.ac.cn; http://iopscience.iop.org/cpb

**What follows is a list of articles you may be interested in**

---

## Ultra-high anisotropy and electronic property of two-dimensional $PbSnS_2$ with a black phosphorus structure

Xinlong Wang(王鑫龙), Shihao Wang(王诗皓), Yandi Jiang(姜彦迪), Qing Min(闵清), Haiming Huang(黄海铭), Chengrui Wu(吴承瑞), and Juntao Yang(杨俊涛)

Chin. Phys. B, 2026, 35 (**5**): 057304. DOI: 10.1088/1674-1056/ae1568

## In-plane negative magnetoresistance and quantum oscillations in van der Waals antiferromagnet $DyTe_3$

Qi Qi(齐琦), Senhao Lv(吕森浩), Ke Zhu(祝轲), Yaofeng Xie(谢耀锋), Guojing Hu(胡国静), Zhen Zhao(赵振), Guoyu Xian(冼国裕), Yechao Han(韩烨超), Yang Yang(杨洋), Lihong Bao(鲍丽宏), Xiao Lin(林晓), Hui Guo(郭辉), Haitao Yang(杨海涛), and Hong-Jun Gao(高鸿钧)

Chin. Phys. B, 2025, 34 (**7**): 077305. DOI: 10.1088/1674-1056/adcc87

## In-plane optical anisotropy of InGaN/GaN quantum disks in nanowires investigated by reflectance difference spectroscopy

Tingting Wei(韦婷婷), Jinling Yu(俞金玲), Zhu Diao, Zhaonan Li(李兆男), Shuying Cheng(程树英), Yunfeng Lai(赖云锋), Yonghai Chen(陈涌海), and Chao Zhao(赵超)

Chin. Phys. B, 2025, 34 (**6**): 067302. DOI: 10.1088/1674-1056/adc6f4

## Nonlinear current response and electric quantum oscillations in the Dirac semimetal $Cd_3As_2$

Hao-Nan Cui(崔浩楠), Ze-Nan Wu(吴泽南), Jian-Kun Wang(王建坤), Guang-Yu Zhu(祝光宇), Jia-Jie Yang(杨佳洁), Wen-Zhuang Zheng(郑文壮), Zhi-Min Liao(廖志敏), Shuo Wang(王硕), Ben-Chuan Lin(林本川), and Dapeng Yu(俞大鹏)

Chin. Phys. B, 2023, 32 (**8**): 087306. DOI: 10.1088/1674-1056/acd9c5

## Tunable charge density wave in $TiS_3$ nanoribbons

Ce Huang(黄策), Enze Zhang(张恩泽), Xiang Yuan(袁翔), Weiyi Wang(王伟懿), Yanwen Liu(刘彦闻), Cheng Zhang(张成), Jiwei Ling(凌霁玮), Shanshan Liu(刘姗姗), Faxian Xiu(修发贤)

Chin. Phys. B, 2017, 26 (**6**): 067302. DOI: 10.1088/1674-1056/26/6/067302

---

**RAPID COMMUNICATION**

# Epitaxial growth of quasi-one-dimensional $TaNi_2Se_2$ monolayer with anisotropic electronic and mechanical properties

Jiayi Wang(王嘉翌)[1,2,†], Qiuchen Yu(余秋辰)[1,2,†], Hui Guo(郭辉)[1,2,†,‡], Peng Fan(范朋)[1,2], Siyu Xu(徐思宇)[1,2], Yixuan Gao(高艺璇)[3,§], Hui Chen(陈辉)[1,2,¶], and Hong-Jun Gao(高鸿钧)[1,2]

[1] *Beijing National Center for Condensed Matter Physics and Institute of Physics, Chinese Academy of Sciences, Beijing* 100190, *China*
[2] *School of Physical Sciences, University of Chinese Academy of Sciences, Beijing* 100190, *China*
[3] *State Key Laboratory for Advanced Metals and Materials, University of Science and Technology Beijing, Beijing* 100083, *China*

(Received 18 March 2026; revised manuscript received 30 March 2026; accepted manuscript online 1 April 2026)

Quasi-one-dimensional (quasi-1D) van der Waals layered materials have garnered significant interest for their intrinsic in-plane anisotropy and potential applications in low-dimensional quantum devices. Here, we report the realization of a quasi-1D $TaNi_2Se_2$ monolayer with pronounced anisotropic electronic and mechanical properties. The monolayer $TaNi_2Se_2$ is synthesized on a graphite substrate via van der Waals epitaxy. Using low-temperature scanning tunneling microscopy/spectroscopy, we reveal the characteristic quasi-1D chain-like lattice structure and confirm the intrinsic metallic nature of the monolayer $TaNi_2Se_2$. Notably, the electronic states exhibit a pronounced quasi-1D modulation that follows the chain structure, indicating strong electronic anisotropy. First-principles calculations further confirm the structural stability and provide signatures of anisotropic in-plane mechanical properties, as well as possible topological edge states arising from spin–orbit coupling. Our findings establish monolayer $TaNi_2Se_2$ as a novel quasi-1D van der Waals material and provide a promising platform for exploring anisotropy-driven quantum phenomena and device applications.

**Keywords:** quasi-1D, $TaNi_2Se_2$ monolayer, anisotropy, epitaxial growth, scanning tunneling microscopy

**PACS:** 73.22.–f, 68.37.Ef, 81.15.Hi, 62.20.de

**DOI:** 10.1088/1674-1056/ae5a15 **CSTR:** 32038.14.CPB.ae5a15

## 1. Introduction

The exploration of two-dimensional (2D) materials has evolved from high-symmetry systems, such as graphene[1–4] and hexagonal transition metal dichalcogenides (TMDs),[5–8] to those exhibiting lower in-plane symmetry, such as black phosphorus,[9,10] $ReS_2$,[11,12] and $WTe_2$.[13,14] Lowering crystal symmetry can introduce new physical degrees of freedom, enabling phenomena such as in-plane anisotropic transport,[15,16] linear dichroism,[17,18] and piezoelectricity.[19,20] Among these low-symmetry materials, a particularly intriguing subclass consists of compounds composed of atomic chains weakly coupled by inter-chain interactions, representing the extreme limit of in-plane anisotropy. These quasi-one-dimensional (quasi-1D) systems bridge the physics of 2D and 1D materials, offering a fertile platform for exploring phenomena associated with reduced dimensionality, including Peierls instability,[21,22] sliding charge density waves (CDWs) in $NbSe_3$,[23,24] CDW-tuned vortex bound states in 1T″-$NbTe_2$,[25] and possible topological superconductivity in $TaSe_3$.[26] Consequently, discovering new quasi-1D van der Waals (vdW) materials has become an important frontier for exploring exotic quantum phases.

Within the family of quasi-1D vdW systems, the ternary chalcogenide family $TaM_2X_2$ ($X$ = Te, Se; $M$ = Ni, Co) is distinguished by its rich phase diagram hosting diverse electronic and magnetic states.[27–32] For instance, $TaNi_2Te_2$ has been identified to exhibit canted antiferromagnetism,[27] while $TaCo_2Te_2$ displays air-stable metallic ferromagnetism with high carrier mobility,[30] as well as large magnetoresistance and quantum oscillations.[29] However, the current studies have predominantly focused on telluride compounds, leaving the selenium-based analogue largely unexplored. Investigating the Te-to-Se substitution is particularly intriguing because the smaller atomic radius of Se effectively introduces a chemical pressure effect.[33] This structural contraction is expected to modify inter-chain hopping and electron correlations, characterized by the ratio between Coulomb interaction and bandwidth (U/W), potentially driving the system toward a quantum ground state distinct from the telluride counterparts.[34,35]

In this work, we report the realization of a quasi-1D $TaNi_2Se_2$ monolayer grown on highly oriented pyrolytic

[†]These authors contributed equally to this work.
[‡]Corresponding author. E-mail: guohui@iphy.ac.cn
[§]Corresponding author. E-mail: gaoyixuan@ustb.edu.cn
[¶]Corresponding author. E-mail: hchenn04@iphy.ac.cn

© 2026 Chinese Physical Society and IOP Publishing Ltd. All rights, including for text and data mining, AI training, and similar technologies, are reserved.

graphite (HOPG) using molecular beam epitaxy (MBE). Low-temperature scanning tunneling microscopy and spectroscopy (STM/STS) measurements reveal the formation of a well-ordered chain-like lattice structure and confirm the intrinsic metallic nature of the monolayer. Remarkably, the electronic states exhibit pronounced quasi-1D modulation following the atomic chains, directly demonstrating strong electronic anisotropy. Combined with first-principles calculations, we further confirm the structural stability of the monolayer and predict anisotropic in-plane mechanical responses, together with possible topological edge states induced by spin–orbit coupling. Our results establish monolayer $TaNi_2Se_2$ as a new member of quasi-1D vdW materials and provide a promising platform for investigating anisotropy-driven quantum phenomena.

## 2. Results and discussion

Figure 1(a) illustrates the crystal structure of the $TaNi_2Se_2$, which crystallizes in an orthorhombic lattice belonging to the space group *Pnma* (No. 62). As shown in the side view model, the $TaNi_2Se_2$ features a sandwich-like structure where a metallic Ta–Ni sub-layer is sandwiched between two selenium atomic sheets. A distinctive structural motif of this phase is the presence of quasi-1D Ta–Ni chains running along the crystallographic *b*-axis. Within these chains, the Ta atoms are coordinated in a distorted monocapped pentagonal prismatic geometry formed by Se atoms,[36] giving rise to a corrugated surface profile. Consequently, the topmost Se atoms occupy two crystallographically inequivalent sites along the *a*-axis.

The monolayer $TaNi_2Se_2$ is grown on a HOPG substrate via vdW epitaxy, a widely used approach for synthesizing 2D layered materials on inert substrates,[37] where the weak interfacial interaction does not require lattice matching while still enabling preferred in-plane orientations.[38–40] In addition, as an inert vdW substrate with minimal coupling, HOPG largely preserves the intrinsic structural and electronic properties of monolayer $TaNi_2Se_2$. Figure 1(b) presents a typical large-scale STM topographic image of the as-grown monolayer $TaNi_2Se_2$. The apparent step height is approximately 0.9 nm, indicating the monolayer thickness. The atomically-resolved STM image shown in Fig. 1(c) reveals a surface morphology dominated by parallel atomic chains. The observed atomic arrangement is consistent with the structural model presented in Fig. 1(a) and resembles the lattice features previously reported in STM studies of $TaNi_2Te_2$ and $TaCo_2Te_2$.[28] To quantitatively determine the lattice periodicity, we performed a fast Fourier transform (FFT) analysis on the atomic-resolution image. The resulting FFT pattern (Fig. 1(d)) exhibits sharp Bragg spots arranged in a rectangular symmetry (marked by blue circles), corroborating the high crystallinity and the orthorhombic symmetry of the $TaNi_2Se_2$. Lattice constants extracted from the line profiles along the principal axes (Fig. 1(e)) yield $a \sim 0.64$ nm and $b \sim 0.36$ nm, in good agreement with the optimized lattice parameters obtained from our density functional theory (DFT) calculations, which give $a = 0.65$ nm and $b = 0.35$ nm for the freestanding monolayer $TaNi_2Se_2$.

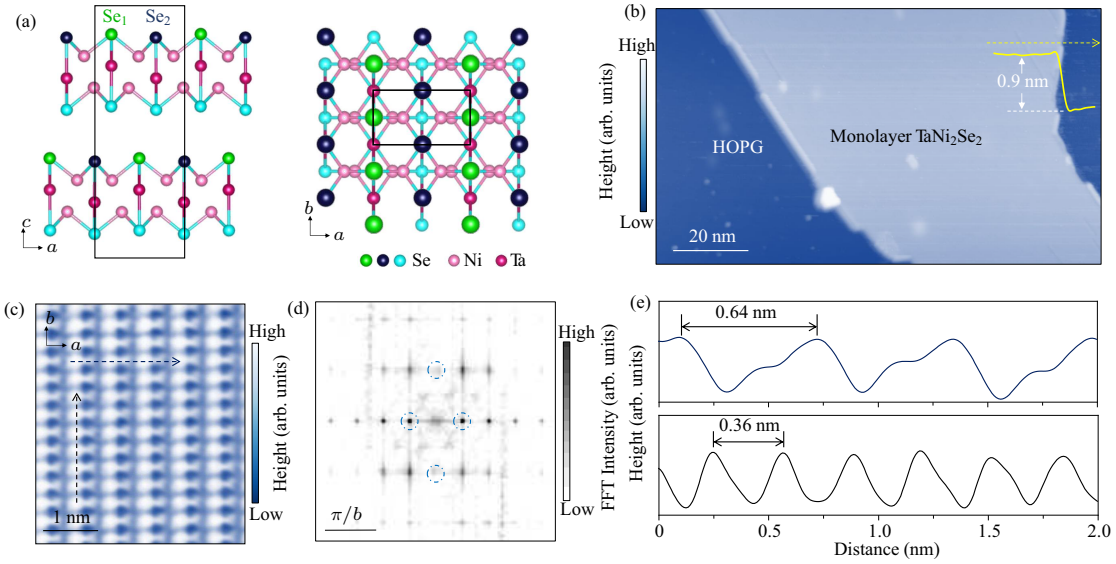



**Fig. 1.** Structural characterizations of monolayer $TaNi_2Se_2$ on HOPG substrate. (a) Side and top views of the crystal structure of $TaNi_2Se_2$, showing a vdW layered structure composed of quasi-1D atomic chains. The topmost Se atoms colored in orange and blue distinguish the two crystallographic inequivalent sites. (b) Large-scale STM topographic image of a monolayer $TaNi_2Se_2$ film ($V_s = 2$ V, $I_t = 100$ pA). The inset displays the height profile measured along the yellow dashed line, showing a step height of approximately 0.9 nm. (c) Atomically-resolved STM image ($V_s = 5$ mV, $I_t = 3$ nA), revealing the quasi-1D lattice structure. (d) The FFT pattern of (c), where the blue circles mark the Bragg diffraction spots arranged in a rectangular symmetry. (e) Height profiles extracted along the white (perpendicular to chains, *a*-axis) and black (parallel to chains, *b*-axis) dashed arrows in (c), yielding lattice constants of $a \sim 0.64$ nm and $b \sim 0.36$ nm, respectively.

We next investigate the electronic properties of the as-grown monolayer $TaNi_2Se_2$. Figure 2(a) presents a typical STM topographic image, where the characteristic chain-like stripes along the *b*-axis are clearly resolved. The $dI/dV$ spectra acquired on two distinct stripes, i.e., the bright and dark stripes, both exhibit a finite density of states at the Fermi level, providing direct experimental evidence of the metallic nature of the monolayer $TaNi_2Se_2$ (Fig. 2(b)). Notably, the relative intensities of the four prominent peaks near the Fermi level, labeled $P_1$–$P_4$, vary significantly between the two distinct stripes. Specifically, the electronic states near $P_1$ and $P_3$ are strongly enhanced on the bright stripe but suppressed on the dark stripe, whereas those near $P_2$ and $P_4$ display the opposite behavior, indicating pronounced spatial modulation of the local electronic states within the unit cell. To visualize the spatial distribution of these electronic states, a $dI/dV$ linecut taken across the stripes exhibits clear periodic modulations within the unit cell (Fig. 2(c)). Importantly, the dominant spectral weight alternates between the energies of $P_2$ and $P_3$ across the unit cell, reflecting the distinct orbital contributions from the alternating Ta–Ni chains and the inequivalent Se environments. In contrast to the linecut across stripes, the $dI/dV$ linecuts taken along both the bright and dark stripes reveal spectral homogeneity, as shown in Figs. 2(d) and 2(e). This pronounced anisotropy, strong modulation across the stripe but homogeneity along them, serves as a spectroscopic signature of the quasi-1D electronic character of the monolayer $TaNi_2Se_2$. Furthermore, the $dI/dV$ maps performed at bias voltages corresponding to peaks $P_3$ (Fig. 2(f)) and $P_2$ (Fig. 2(g)) reveal strongly localized stripe-like electronic features and energy-dependent contrast reversal, further reflecting highly anisotropic electronic states confined by the quasi-1D structural chains.

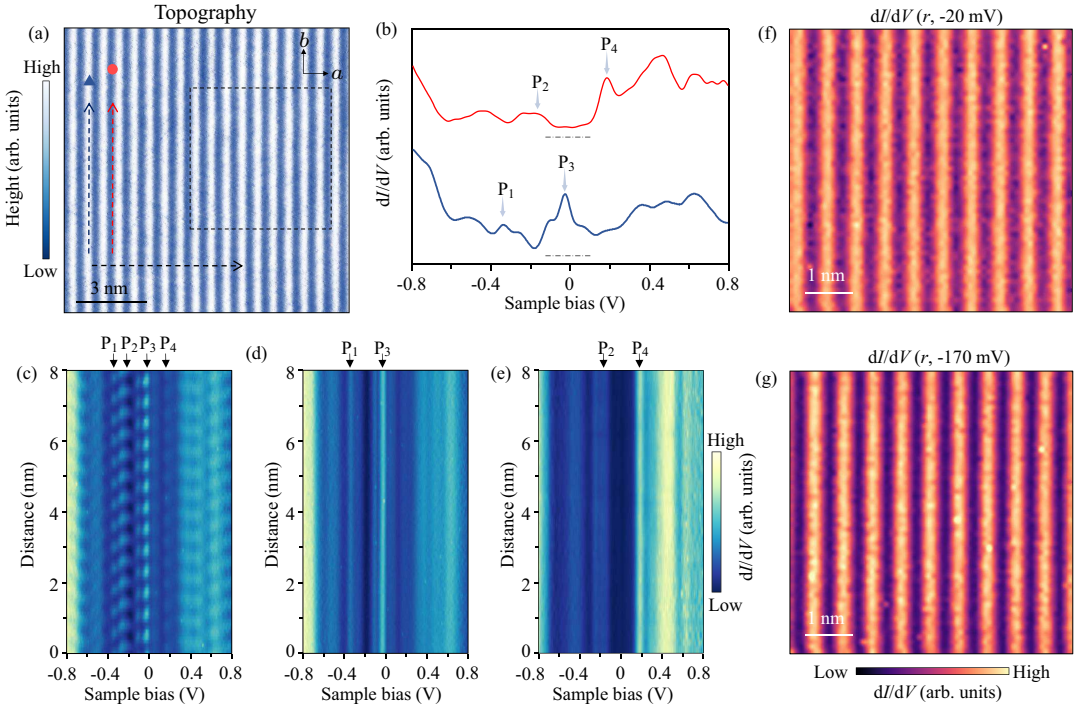



**Fig. 2.** Anisotropic electronic properties of the monolayer $TaNi_2Se_2$. (a) STM topography, showing the quasi-1D stripe-like structure characteristics ($V_s = -400$ mV, $I_t = 1.9$ nA). (b) The $dI/dV$ spectra acquired at the bright stripe (blue curve, position marked by blue triangle in (a)) and dark stripe (red curve, position marked by red circle in (a)), showing pronounced difference of the electronic states between the two kinds of stripes. Four characteristic peaks are labeled as $P_1$–$P_4$. The zero $dI/dV$ position is indicated by the black dashed lines. (c) The $dI/dV$ linecut taken across the stripes (black dashed arrow in (a)), showing a strong periodic modulation of the electronic states across the bright and dark stripes. (d), (e) The $dI/dV$ linecuts taken along the bright stripe (blue dashed arrow in (a)) and dark stripe (red dashed arrow in (a)), respectively, both showing spatial homogeneity of the electronic states. (f), (g) The $dI/dV$ maps acquired in the region marked by the black square in (a), at energies corresponding to peaks $P_3$ (f) and $P_2$ (g), respectively, showing energy-dependent contrast reversal.

To gain deep insight into the intrinsic properties of monolayer $TaNi_2Se_2$, we further performed DFT calculations. To evaluate the structural stability of the monolayer, we calculated the phonon dispersion spectrum, as shown in Fig. 3(a). The absence of imaginary frequencies throughout the Brillouin zone confirms the dynamical stability of the monolayer $TaNi_2Se_2$, consistent with the successful experimental realization of the material. Figure 3(b) presents the calculated electronic band structure of the freestanding monolayer $TaNi_2Se_2$ without SOC. Multiple bands cross the Fermi level, indicating a metallic ground state, in good agreement with the STS measurements. The metallic behavior mainly arises from the transition metal d-orbitals forming dispersive states near the Fermi level.[29] Notably, a saddle-point-like band feature appears near the *Y* point in the vicinity of the Fermi level, which is expected to induce an enhanced density of states and may

contribute to the peak structure ($P_3$) observed in the STS spectra in Fig. 2(b). When SOC is included, the band structure exhibits noticeable modifications. As shown in Fig. 3(c), SOC lifts the band degeneracy and induces a local energy gap opens at the $\Gamma$ point approximately 1 eV above the Fermi level (highlighted by the blue dashed box). This gap opening can be attributed to the band anti-crossing effect induced by the strong spin–orbit interaction inherent to the heavy Ta 5d orbitals. We further calculate the edge states using a semi-infinite monolayer $TaNi_2Se_2$. The projected edge band structure (Fig. 3(d)) exhibits emergent edge states that bridges the bulk valence and conduction bands. The appearance of such conducting channels within the SOC gap suggests the existence of topological boundary states. However, the edge-state energy range significantly overlaps with bulk bands rather than residing in a clean global gap, causing the edge contribution to be masked by the bulk density of states and hindering unambiguous experimental identification.

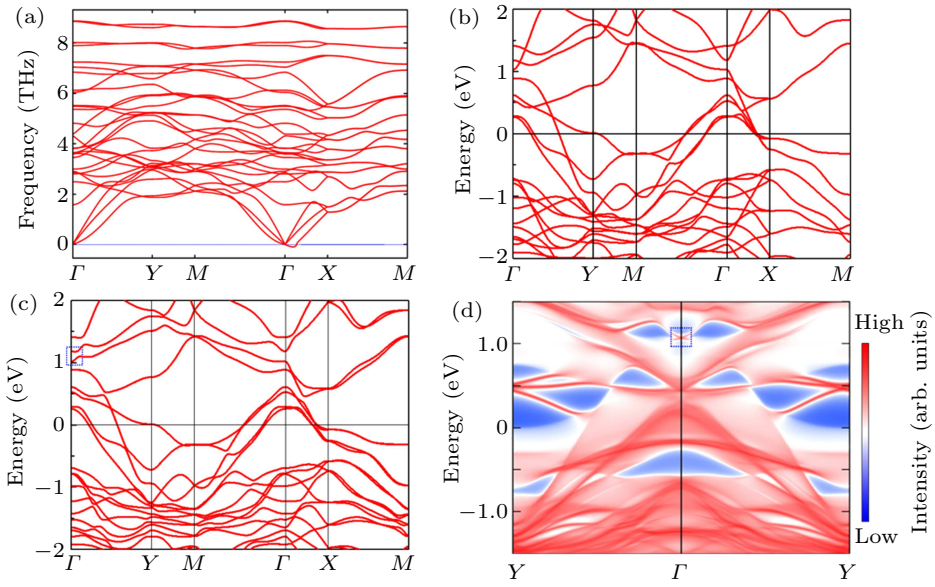



**Fig. 3.** Theoretical calculations of the stability and electronic structure of freestanding monolayer $TaNi_2Se_2$. (a) Phonon dispersion spectrum calculated along high-symmetry paths. The absence of imaginary frequencies across the entire Brillouin zone confirms the dynamic stability of the monolayer $TaNi_2Se_2$. (b) Electronic band structure calculated without SOC. The bands crossing the Fermi level $E_F$ indicate a metallic ground state, consistent with the experimental $dI/dV$ measurements. (c) The calculated band structure with SOC, showing an energy gap opening at the $\Gamma$ point approximately 1 eV above the Fermi level (marked by the blue dashed box). (d) Projected edge states using a semi-infinite $TaNi_2Se_2$ model, showing emergence of edge states within the SOC-induced gap, bridging the bulk valence and conduction bands (highlighted by the blue dashed rectangle).

Finally, we evaluate the mechanical properties of the quasi-1D monolayer $TaNi_2Se_2$ by calculating its orientation-dependent elastic constants using DFT. For a 2D orthorhombic system, there are four independent elastic constants: $C_{11}$, $C_{22}$, $C_{12}$, $C_{66}$. Our results show that these constants satisfy the Born criteria, namely $C_{11}C_{22} - C_{12}^2 > 0$ and $C_{11}, C_{22}, C_{66} > 0$, providing further evidence for the mechanical stability of the $TaNi_2Se_2$ monolayer, consistent with the phonon dispersion results. Based on these elastic constants, the orientation-dependent Young's modulus $E(\theta)$, shear modulus $G(\theta)$, and Poisson's ratio $\nu(\theta)$ can be obtained using the following equations:

$$E(\theta) = \frac{1}{s_{11}c^4 + (2s_{12} + s_{66})s^2c^2 + s_{22}s^4},$$

$$G(\theta) = \frac{1}{4s_{11}s^2c^2 + 4s_{22}s^2c^2 + 8s_{12}s^2c^2 + s_{66}(s^2 - c^2)^2},$$

$$\nu(\theta) = -\frac{s_{12}(s^4 + c^4) + (s_{11} + s_{22} - s_{66})s^2c^2}{s_{11}c^4 + (2s_{12} + s_{66})s^2c^2 + s_{22}s^4},$$

where $c = \cos(\theta)$ and $s = \sin(\theta)$; $s_{11}$, $s_{22}$, $s_{12}$, and $s_{66}$ are the compliance constants derived from the elastic constant matrix.

As illustrated in Fig. 4, monolayer $TaNi_2Se_2$ exhibits pronounced in-plane mechanical anisotropy. The orientation-dependent Young's modulus $E(\theta)$, shear modulus $G(\theta)$ and Poisson's ratio $\nu(\theta)$ vary nonmonotonically as the direction rotates from $\theta = 0°$ to 90°. Specifically, the Young's modulus increases from 98.8 N/m at 0° to a maximum of 124.2 N/m at 45°, and then decreases to 76.8 N/m at 90°. In contrast, the shear modulus decreases from 48.6 N/m at 0° to 29.4 N/m at 45°, before recovering to 48.6 N/m at 90°. Meanwhile, the Poisson's ratio decreases from 0.54 to 0.25 between 0° and 45°, and then increases to 0.42 at 90°. The intrinsic Young's modulus of monolayer $TaNi_2Se_2$ is lower than those of conventional TMDs[41] but higher than that of anisotropic 2D materials such as black phosphorus ($\sim$ 44 N/m).[42] The combination of relatively high shear rigidity and axial tensile compliance originates from quasi-1D Ta–Ni chain framework, highlighting its potential for application in flexible and strain-engineered nanodevices.

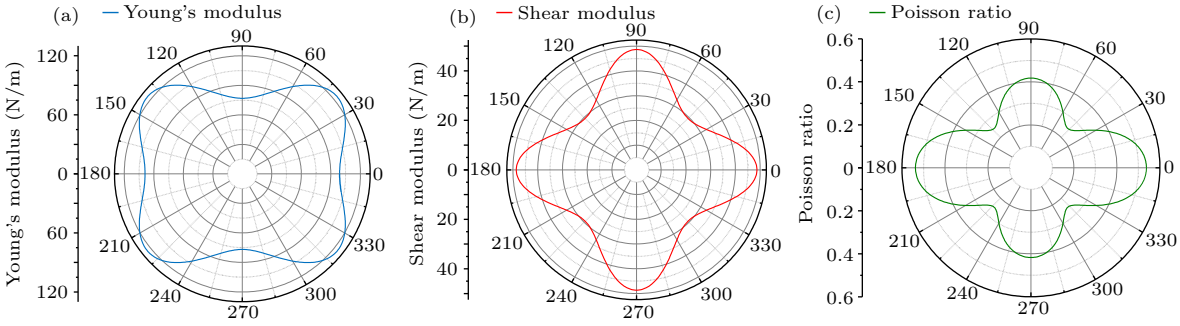



**Fig. 4.** Calculated anisotropic in-plane mechanical properties of monolayer $TaNi_2Se_2$. (a)–(c) Polar plots of Young's modulus $E(\theta)$ (a), shear modulus $G(\theta)$ (b), and Poisson's ratio $\nu(\theta)$ (c), showing pronounced mechanical anisotropy of the $TaNi_2Se_2$. The initial angle $\theta = 0°$ corresponds to the crystallographic $a$-axis.

## 3. Conclusions

We have successfully synthesized quasi-1D monolayer $TaNi_2Se_2$ via molecular beam epitaxy. Low-temperature STM imaging reveals its characteristic quasi-1D chain-like lattice, while STS measurements confirm the intrinsic metallic nature of the monolayer. Notably, spatially resolved spectroscopy uncovers a pronounced quasi-1D modulation of the electronic states following the chain structure, demonstrating strong electronic anisotropy. First-principles calculations further verify the structural stability of monolayer $TaNi_2Se_2$ and reveal pronounced in-plane mechanical anisotropy, as well as possible topological edge states induced by SOC. These results establish monolayer $TaNi_2Se_2$ as a promising quasi-1D vdW material with coupled electronic and mechanical anisotropy, providing a potential platform for future applications in direction-dependent nanomechanical devices[43] or strain-engineered systems.[44,45]

## Appendix A: Experimental methods

**Sample preparation** Monolayer $TaNi_2Se_2$ is epitaxially grown on HOPG substrates in an ultra-high-vacuum (UHV) MBE system (base pressure $\sim 5 \times 10^{-10}$ mbar). High-quality HOPG substrate with atomically flat surfaces is obtained by mechanical exfoliation followed by degassing at $\sim$ 870 K for several hours. The monolayer $TaNi_2Se_2$ is grown by co-evaporating Ta (99.9%, Goodfellow Cambridge Ltd.), Ni (99.95%, Goodfellow Cambridge Ltd.), and Se (99.99%, Sigma-Aldrich) atoms with the substrate maintained at 893 K. The substrate temperature and the Ta/Ni flux ratio must be controlled within an optimized growth window to suppress the formation of other competing quasi-one-dimensional Ta–Ni–Se compounds and thereby obtain a pure $TaNi_2Se_2$ phase. During growth, the Se flux is kept approximately one order of magnitude higher than the Ta and Ni fluxes to ensure a Se-rich atmosphere. After growth, the sample is kept at 523 K for 30 minutes to remove additional Se.

**STM/STS characterizations** After the sample growth, it is then transferred to an STM system via a home-made UHV suitcase. The STM experiments are carried out at 4.1 K in an ultrahigh vacuum ($1 \times 10^{-11}$ mbar) LT-STM systems in the constant current mode with a tungsten tip, which is calibrated on a clean Au(111) surface. STS are acquired by a standard lock-in amplifier at a frequency of 973.1 Hz, under the modulation voltage $V_{\text{mod}} = 20$ mV.

**DFT calculations** The calculations of monolayer $TaNi_2Se_2$ are carried out by using Vienna *ab initio* simulation package (VASP) with the projector augmented wave (PAW) method.[46] A generalized gradient approximation (GGA) in the form of Perdew–Burke–Ernzerhof (PBE) is adopted for the exchange–correlation functional.[47] A 20 Å vacuum layer is used, and all atoms are fully relaxed until the residual forces on each atom are smaller than 0.01 eV/Å. The $k$-points sampling is $12 \times 24 \times 1$ with the Gamma scheme. Wave functions were expanded on a plane-wave basis set up to 500 eV energy cutoff. The fully relaxed lattice constant of monolayer $TaNi_2Se_2$ is 6.472 Å, 3.452 Å in $a$ and $b$ direction, respectively. The Wannier functions are constructed using the WANNIER90 code.[48] The edge-state calculations based on Wannier functions were done using the WannierTools package.[49] Phonon dispersion is calculated based on supercells larger than 19 Å in the density-functional perturbation theory method implemented in the PHONOPY package.[50]

## Acknowledgements

This work is supported by the National Key Research and Development Program of China (Grant No. 2022YFA1204100), the National Natural Science Foundation of China (Grant Nos. 62488201, 92580202, 52572188, 52572063, and 52350322), the CAS Project for Young Scientists in Basic Research (Grant Nos. YSBR-053 and YSBR-003), the Fundamental Research Funds for the Central Universities (Grant Nos. FRF-TP-24-055A and FRF-IDRY-24-007), and the State Key Lab for Advanced Metals and Materials (Grant Nos. 41601124 and 41601126).

## References

[1] Novoselov K S, Geim A K, Morozov S V, Jiang D, Katsnelson M I, Grigorieva I V, Dubonos S V and Firsov A A 2005 *Nature* **438** 197

[2] Zhang Y, Tan Y W, Stormer H L and Kim P 2005 *Nature* **438** 201
[3] Pan Y, Zhang H, Shi D, Sun J, Du S, Liu F and Gao H J 2009 *Adv. Mater.* **21** 2777
[4] Guo H, Zhang R, Li H, Wang X, Lu H, Qian K, Li G, Huang L, Lin X, Zhang Y, Ding H, Du S X, Pantelides S T, Gao H J 2020 *Nano Lett.* **20** 2674
[5] Ye J T, Zhang Y J, Akashi R, Bahramy M S, Arita R and Iwasa Y 2012 *Science* **338** 1193
[6] Geim A K and Grigorieva I V 2013 *Nature* **499** 419
[7] Guo H, Huang Z, Gao Y, Chen H, Zhang H, Fang Q, Ye Y, Han X, Cao Z, Wang J, Zhou R, Li Z, Shen C, Yang H, Chen H, Yao W, Wang Z and Gao H J 2025 *Nat. Commun.* **16** 11327
[8] Liu Z L, Wu X, Shao Y, Qi J, Cao Y, Huang L, Liu C, Wang J O, Zheng Q, Zhu Z L, Ibrahim K, Wang Y L and Gao H J 2018 *Sci. Bull.* **63** 419
[9] Kim J, Baik S S, Ryu S H, Sohn Y, Park S, Park B G, Denlinger J, Yi Y, Choi H J and Kim K S 2015 *Science* **349** 723
[10] Wang G, Bao L, Pei T, Ma R, Zhang Y Y, Sun L, Zhang G, Yang H, Li J, Gu C, Du S, Pantelides S T, Schrimpf R D and Gao H J 2016 *Nano Lett.* **16** 6870
[11] Tongay S, Sahin H, Ko C, Luce A, Fan W, Liu K, Zhou J, Huang Y S, Ho C H, Yan J, Ogletree D F, Aloni S, Ji J, Li S, Li J, Peeters F M and Wu J 2014 *Nat. Commun.* **5** 3252
[12] Chenet D A, Aslan B, Huang P Y, Fan C, van der Zande A M, Heinz T F and Hone J C 2015 *Nano Lett.* **15** 5667
[13] Ali M N, Xiong J, Flynn S, Tao J, Gibson Q D, Schoop L M, Liang T, Haldolaarachchige N, Hirschberger M, Ong N P and Cava R J 2014 *Nature* **514** 205
[14] Zhu Y, Wang Z, Ren Y, Yuan P, Chen J, Ou Y, Meng L and Zhang Y 2025 *Chin. Phys. B* **34** 017302
[15] Lin Y C, Komsa H P, Yeh C H, Björkman T, Liang Z Y, Ho C H, Huang Y S, Chiu P W, Krasheninnikov A V and Suenaga K 2015 *ACS Nano* **9** 11249
[16] Zhou K, Deng J, Chen L, Xia W, Guo Y, Yang Y, Guo J G and Guo L 2021 *Chin. Phys. B* **30** 087202
[17] Wang X, Jones A M, Seyler K L, Tran V, Jia Y, Zhao H, Wang H, Yang L, Xu X and Xia F 2015 *Nat. Nanotechnol.* **10** 517
[18] Aslan B, Chenet D A, van der Zande A M, Hone J C and Heinz T F 2016 *ACS Photonics* **3** 96
[19] Wu W, Wang L, Li Y, Zhang F, Lin L, Niu S, Chenet D, Zhang X, Hao Y, Heinz T F, Hone J and Wang Z L 2014 *Nature* **514** 470
[20] Zhu H, Wang Y, Xiao J, Liu M, Xiong S, Wong Z J, Ye Z, Ye Y, Yin X and Zhang X 2015 *Nat. Nanotechnol.* **10** 151
[21] Hellmann S, Rohwer T, Kalläne M, Hanff K, Sohrt C, Stange A, Carr A, Murnane M M, Kapteyn H C, Kipp L, Bauer M and Rossnagel K 2012 *Nat. Commun.* **3** 1069
[22] Huber T, Mariager S O, Ferrer A, Schäfer H, Johnson J A, Grübel S, Lübcke A, Huber L, Kubacka T, Dornes C, Laulhe C, Ravy S, Ingold G, Beaud P, Demsar J and Johnson S L 2014 *Phys. Rev. Lett.* **113** 026401
[23] Brun C, Wang Z Z, Monceau P and Brazovskii S 2010 *Phys. Rev. Lett.* **104** 256403
[24] van Midden M A, van Midden H J P, Prodan A, Bennett J C and Zupanič E 2020 *Phys. Rev. B* **102** 075442
[25] Zhang H, Chen H, Huang Z, Wang Z A, Lv S, Xian G, Guo H, Yang H and Gao H J 2025 *Nano Lett.* **25** 16650
[26] Liu S, Nie S M, Qi Y P, Guo Y F, Yuan H T, Yang L X, Chen Y L, Wang M X and Liu Z K 2021 *Chin. Phys. Lett.* **38** 077302
[27] Tan H, Feng Y, Ma X, Wang C, Li R, Wu J, Huang L, Lu Y and Xiang B 2024 *Phys. Rev. Mater.* **8** 104412
[28] Neuhausen J, Evstaf'iev V K, Block T, Finckh E W, Tremel W, Augustin L, Fuchs H, Voß D, Krüger P, Mazur A and Pollmann J 1998 *Chem. Mater.* **10** 3870
[29] Jiao W H, Liu Y, Tao P, Lu J, Liang X, Yang W, Zhang Z, Xu S, Luo Y, Zhu Z W, Qian D, Xu X, Ren Z, Cao G H and Xiao S 2025 *Phys. Rev. B* **111** 045109
[30] Singha R, Yuan F, Cheng G, Salters T H, Oey Y M, Villalpando G V, Jovanovic M, Yao N and Schoop L M 2022 *Adv. Funct. Mater.* **32** 2108920
[31] Wang L, Tian J, Kang C, Gu H, Pang R, Shen M, She L, Song Y, Liu X and Zhang W 2022 *Inorg. Chem.* **61** 18899
[32] Pate S, Chen B, Shen B, Li K, Zhou X, Chung D Y, Divan R, Kanatzidis M G, Welp U, Kwok W K and Xiao Z L 2024 *Phys. Rev. B* **109** 035129
[33] Chhowalla M, Shin H S, Eda G, Li L J, Loh K P and Zhang H 2013 *Nat. Chem.* **5** 263
[34] Yin Z P, Haule K and Kotliar G 2011 *Nat. Mater.* **10** 932
[35] Imada M, Fujimori A and Tokura Y 1998 *Rev. Mod. Phys.* **70** 1039
[36] Huang J 2000 *Sc. China Ser. B-Chem.* **43** 337
[37] Koma A 1992 *Thin Solid Films* **216** 72
[38] Yu Y, Wang G, Qin S, Wu N, Wang Z Y, He K and Zhang X A 2017 *Carbon* **115** 526
[39] Huang X, Guan J, Lin Z, Liu B, Xing S, Wang W and Guo J 2017 *Nano Lett.* **17** 4619
[40] Yu Y, Wang G, Tan Y, Wu N, Zhang X A and Qin S 2018 *Nano Lett.* **18** 675
[41] Zeng F, Zhang W B and Tang B Y 2015 *Chin. Phys. B* **24** 097103
[42] Wei Q and Peng X 2014 *Appl. Phys. Lett.* **104** 251915
[43] Wang Z, Jia H, Zheng X Q, Yang R, Ye G J, Chen X H and Feng P X L 2016 *Nano Lett.* **16** 5394
[44] Qin M S, Zhu P F, Ye X G, Xu W Z, Song Z H, Liang J, Liu K and Liao Z M 2021 *Chin. Phys. Lett.* **38** 017301
[45] Ryu Y K, Carrascoso F, López-Nebreda R, Agraït N, Frisenda R and Castellanos-Gomez A 2020 *Nano Lett.* **20** 5339
[46] Kresse G and Furthmüller J 1996 *Phys. Rev. B* **54** 11169
[47] Perdew J P, Burke K and Ernzerhof M 1996 *Phys. Rev. Lett.* **77** 3865
[48] Mostofi A A, Yates J R, Pizzi G, Lee Y S, Souza I, Vanderbilt D and Marzari N 2014 *Comput. Phys. Commun.* **185** 2309
[49] Wu Q, Zhang S, Song H F, Troyer M and Soluyanov A A 2018 *Comput. Phys. Commun.* **224** 405
[50] Togo A and Tanaka I 2015 *Scr. Mater.* **108** 1